# Cracking quantification of wood exposed to constant heat fluxes

Boris Aguilar, Pedro Reszka, Zoubir Acem, Pascal Boulet, Gilles Parent, Lucas Terrei

Fire Safety Journal 158 (2025) 104546

Contents lists available at ScienceDirect

Fire Safety Journal

journal homepage: www.elsevier.com/locate/firesaf

# Cracking quantification of wood exposed to constant heat fluxes

Boris Aguilar [a], Pedro Reszka [b], Zoubir Acem [c], Pascal Boulet [c], Gilles Parent [c], Lucas Terrei [c,*]

[a] Institut de Mécanique des Fluides de Toulouse (IMFT), Université de Toulouse, CNRS-INPT-UPS, Toulouse, 31400, France
[b] Facultad de Ingeniería y Ciencias, Universidad Adolfo Ibáñez, Avda. Diagonal Las Torres 2640, Santiago, 7941169, Chile
[c] Université de Lorraine, CNRS, LEMTA, Nancy, F-54000, France

ARTICLE INFO

*Keywords:*
Cracks
Wood
Infrared camera
Cone calorimeter

ABSTRACT

Surface cracking of wood when exposed to a heat source is one of the factors understudied by the fire community despite the fact that the cracks may guide the release of pyrolysis gases, inducing heterogeneity in the effusion of gas and therefore may affect ignition and extinction of flame at the material surface. This study aimed to develop a dynamic detection method for characterizing wood cracking during fire tests by providing quantities such as surface area, length, and number of cracks. Spruce samples were exposed to a wide range of heat fluxes during for at least 40 min using a vertical cone calorimeter. An infrared camera with a specific filter wavelength was used to track crack formation. A total of 74 experiments were carried out in air, and seven were carried out in an oxygen-free atmosphere to determine the cracking dynamics of the wood. The results show that the cracking rate and the number of cracks quickly reach to a constant value. The heat flux and the presence of oxygen are not dominant factors in wood's dynamic cracking. This work provides quantitative data for readers interested in accounting for cracking and heterogeneous pyrolysis gas release on the surface of a sample.

## 1. Introduction

Several well-known processes occur when wood is exposed to fire. First, the wood dries. As the temperature continues to rise, pyrolysis reactions begin. These reactions are numerous and complex. As the wood transforms into char, small cracks form. The intensity of the incident heat flux at the surface, wood species, and moisture content are a few factors influencing these processes, as discussed in Drysdale's book [1]. Cracks also play a significant role in the possible ignition of wood. Indeed, when the heat flux is close to the critical heat flux for ignition, auto-ignition occurs after a more or less long time depending on the release of flammable pyrolysis gases. Ignition then takes place at the point where the pyrolysis gases are released from the wood surface, in the vicinity of the cracks [2–5]. Depending on their geometry, cracks can modify how the wood is heated by allowing radiation to reach deeper parts of the sample. Cracks are also responsible for the conditions that enable wood to self-extinguish since they assist in maintaining the flame [6]. Therefore, cracks play an important role in increasing the local heat flux and releasing volatiles in all these combustion processes, and this should be considered when modeling and studying the fire behavior of wood. Since numerical modeling of wood pyrolysis and combustion in fires began in 1946 [7], there is an overall consensus on the role of cracks in these processes. However, cracks are not commonly considered in recent pyrolysis models [8].

A crack is a discontinuity in wood caused by external thermal stress that fragments the char over a defined surface area. The appearance of cracks is linked to the fibrous nature of cellulose and lignin fibers. According to Baroudi et al. cracks appear due to the tube arrangement which can induce thermomechanical instability, drying shrinkage, and specimen deformations [9]. The notion of internal stress to account for cracking during wood combustion is also the basis of recent modeling works of Wichman et al. and Zhang et al. [10,11]. Wichman et al. demonstrated that boundary conditions at the edges and the initial geometry of the sample, particularly its thickness, influence crack progression. However, few of these studies compare modeling results with experimental results, due to the lack of precise data. Shen et al. argue that the cracking mechanism occurs during pyrolysis [12]. It is believed to result from the breaking of chemical bonds between carbon atoms and polymer chains. Conrad et al. showed three modes of cracking depending on the grain orientation [13].

Experimental work on wood cracking has not reached a consensus on the dominant factor influencing crack formation. At the macro TGA scale, Kwiatkowski et al. concluded that char fragmentation does not play an important role in heat transfer [14]. However, this observation was made in an inert atmosphere, so more accurate prediction of heat transfer would require knowledge of the effect of the environment on wood cracking. Li et al. exposed fir and medium-density fiberboard

* Corresponding author.
*E-mail address:* lucas.terrei@univ-lorraine.fr (L. Terrei).

https://doi.org/10.1016/j.firesaf.2025.104546
Received 30 June 2025; Received in revised form 17 September 2025; Accepted 19 September 2025
Available online 26 September 2025

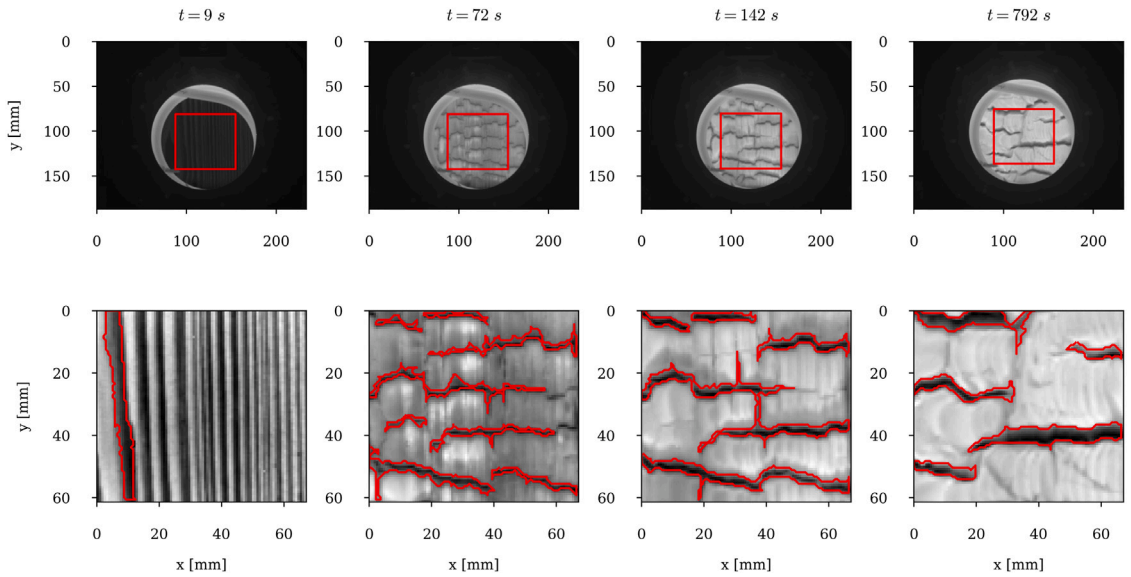


**Fig. 1.** Infrared images and detection of the studied zone during wood cracking exposed to 55 kW·m$^{-2}$. The top row shows the raw images, and the bottom row shows the normalized images from the window of interest. (For interpretation of the references to color in this figure legend, the reader is referred to the web version of this article.)

to different heat fluxes and atmospheres. They demonstrated that a combination of high heat flux and low ambient pressure increases the number of cracks [15,16]. Chu et al. studied the crack formation of densified pine wood using a cone calorimeter at three heat fluxes with a maximum exposure time of 600 seconds [17,18]. The authors analyzed two types of cracks, longitudinal and tangential to the fiber directions. The number of cracks was defined and averaged across three lines of the samples. The number of cracks before oxidation increases with the applied heat flux; however, there is no clear trend at the end of the experiment [17]. Shen et al. showed that there was an increase in cracking from 15 to 50 kW·m$^{-2}$ and that this cracking increased with the heating time. Moreover, Shen et al. showed that the cracking was dependent on the wood species with a greater cracking for softwood [12]. Rinta-Paavola et al. and Baroudi et al. found no trend between the heat flux and the number of cracks for different wood species in inert atmospheres [9,19]. However, most of these studies do not provide the evolution over time of the cracking phenomenon. They are mainly based on post-test observations, and the results may also differ according to the cooling process.

The state of the art shows that the specific study of wood cracking during combustion is quite recent and limited, and does not lead to unanimous conclusions. For instance, there is no consensus on how the incident heat flux affects crack formation, cracking rates, and morphology. Recent research on wood cracking during thermal decomposition sheds new light on the phenomenon and provides information such as the number of cracks on specimens at specified times during heating [9,17–19]. However, the methods used to determine the evolution of crack number and size are never explicitly described. This suggests that the experimenter manually determined the cracks and that the results are mainly based on experimental observation. These techniques do not allow for the tracking of crack parameters over time. More recently, Chu et al. proposed observing the cracking of a pine sample using infrared with an experimental device [20]. The authors showed the evolution of the surface area, total length, and average thickness of the cracks for two pine samples subjected to a heat flux of 30 kW·m$^{-2}$.

Discrepancies between degradation models and experiments suggest the possible effect of cracking, but there is little characterization data to confirm or refute this hypothesis. One possible explanation is that gas effusion is heterogeneous and could affect the flammability and extinction conditions on the surface. Therefore, it is important to characterize cracking and verify the effect of operating conditions, such as time, incident heat flux intensity, and oxidizing or non-oxidizing conditions. However, quantifying cracking is difficult because it requires interrupting a degradation test and quickly cooling the sample to preserve its structure. These tests must be repeated many times with different heat fluxes. Only then can we analyze the cracks in these often fragile structures. The present work proposes a new method to analyze the dynamic behavior of spruce samples exposed during 60 min to different incident heat fluxes (from 20 to 85 kW·m$^{-2}$) from a cone calorimeter in vertical orientation. The samples chosen were 50 mm thick, to avoid any potential problems related to the progression of the pyrolysis front in the wood, and to enable experiments to be carried out over long periods. The method uses infrared imaging processing with a specific wavelength filter for which the flame is almost transparent and does not disturb the image of the wood surface. This method enables the detailed quantification of specimen evolution in terms of crack surface ratio, number of cracks, and crack characteristic length. Finally, a comparative study was conducted in an inert chamber to quantify spruce cracking with and without oxygen and to examine the impact of char oxidation on cracking dynamics.

## 2. Materials and methods

### 2.1. Experimental setup

The experiments were carried out using a vertical cone calorimeter without a pilot. The samples were placed in a steel sample holder 25 mm away from the cone coil. The heat fluxes studied were $\dot{q}''_{inc}$ = 20, 35, 45, 55, 75, and 85 kW·m$^{-2}$ and the exposure times ranged from 40 to 60 minutes [3]. The wood species was spruce with a moisture content between 9 and 11%. The samples' density varied between 400 and 550 kg·m$^{-3}$ and the grain orientation was perpendicular to the heat flux with fibers always vertical. Note that the 10 × 10 cm$^2$ and 5 cm thick specimens were cut from large glulam panels composed of 5 cm wide battens; consequently, the specimens have at least one glued joint [21]. The joints were kept vertical, and any fissures caused by delamination in the joint were not considered in the analysis, which focused on cracking in the solid wood. Table 1 presents the number of tests (74 in total) for the different heat fluxes.

These tests were all carried out in air to study the effect of heat flux on wood cracking. A second series of experiments was conducted under identical conditions, but in a controlled atmosphere chamber.

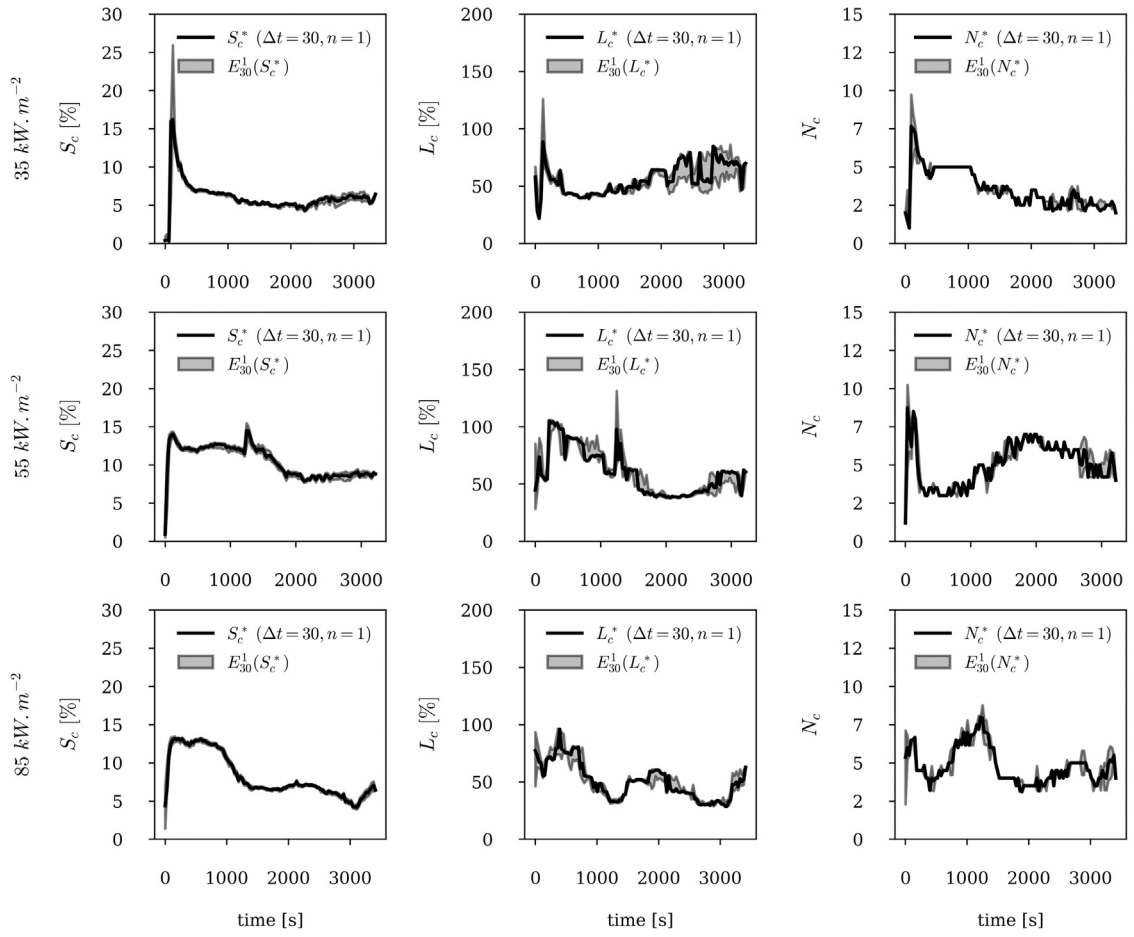


**Fig. 2.** Crack ratio, characteristic length and number of cracks according to the imposed heat flux.

**Table 1**
Experimental campaign in air atmosphere.

| Heat flux (kW·m$^{-2}$) | 20 | 35 | 45 | 55 | 75 | 85 |
|---|---|---|---|---|---|---|
| Number of tests | 7 | 5 | 28 | 12 | 13 | 9 |

The spruce samples were placed in a steel chamber where oxygen was removed with a constant flow of argon at a rate of 10 L·min$^{-1}$ [22,23]. The samples were exposed to 35 kW·m$^{-2}$ (four tests) and 45 kW·m$^{-2}$ (three tests) for 20 min. To stop the degradation process, all samples were immediately cooled down after the test by pouring liquid nitrogen onto them.

An infrared camera (FLIR Orion SC7000) was used to visualize the cracks and measure the surface temperature of the samples during testing [3]. The camera has a resolution of 320 × 256 pixels, and its sensor is an InSb detector. The camera was aligned with the cone axis and placed 50 cm behind the cone to measure the temperature through the cone coil's aperture. Under these conditions, one pixel in the image corresponds to 730 μm. The camera is equipped with a bandpass filter at a wavelength of 3.9 μm (2564 cm$^{-1}$), which is outside the emission bands of combustion gases ($CO_2$ and $H_2O$) [24]. With this device and at this scale, the flame between the wood surface and the camera has a very small optical thickness and can be considered transparent at this wavelength. Before the tests, the camera was calibrated with a black-body to determine the relationship between the measured signal and intensity. The frame rate was 50 Hz, and 16 frames were subsampled, resulting in an image recorded every 0.32 s. From these measurements, a comprehensive set of surface temperatures was obtained for each test mentioned in Refs. [25,26]. It should be noted that detecting cracks during the test with a visible camera would have been more difficult, as the flame would have interfered with the analysis.

### 2.2. Infrared image processing

Fig. 1 shows an example of infrared images recorded at a heat flux of 55 kW·m$^{-2}$ at four different times. These times were chosen to illustrate the various stages of the cracking process and the crack detection code's operation. At $t$ = 9 s, it is possible to observe the presence of the heating coil of the cone. For this reason, a window of interest measuring approximately 60 × 60 mm$^2$ was defined. This window is represented by the red rectangle in each image of the first row. In the second row of Fig. 1, the images are normalized between the minimum and maximum digital values of the window of interest. We developed a contour detection algorithm based on adaptive thresholding (the `opencv` Python function) for each image to detect the cracks circled in red. In the first image of the second row of Fig. 1, at $t$ = 9 s, the wood grain patterns clearly appear within the region of interest, as they exhibit an emissivity different from that of the surrounding wood. Across all test points in the study, these grain patterns remain visible for up to 30 s after exposure begins. To prevent their contours from being detected and mistakenly classified as cracks, exclusion criteria were established. If a detected contour's bounding rectangle has a length greater than 80% of the image height, a width less than 10% of the image width, and an orientation between 85 and 95 degrees, the contour is classified as a grain pattern and excluded from the analysis. However, this method does not guarantee the strict exclusion of all grain patterns, as demonstrated in the region of interest at $t$ = 9 s. For the remainder of the study, the descriptors extracted from the

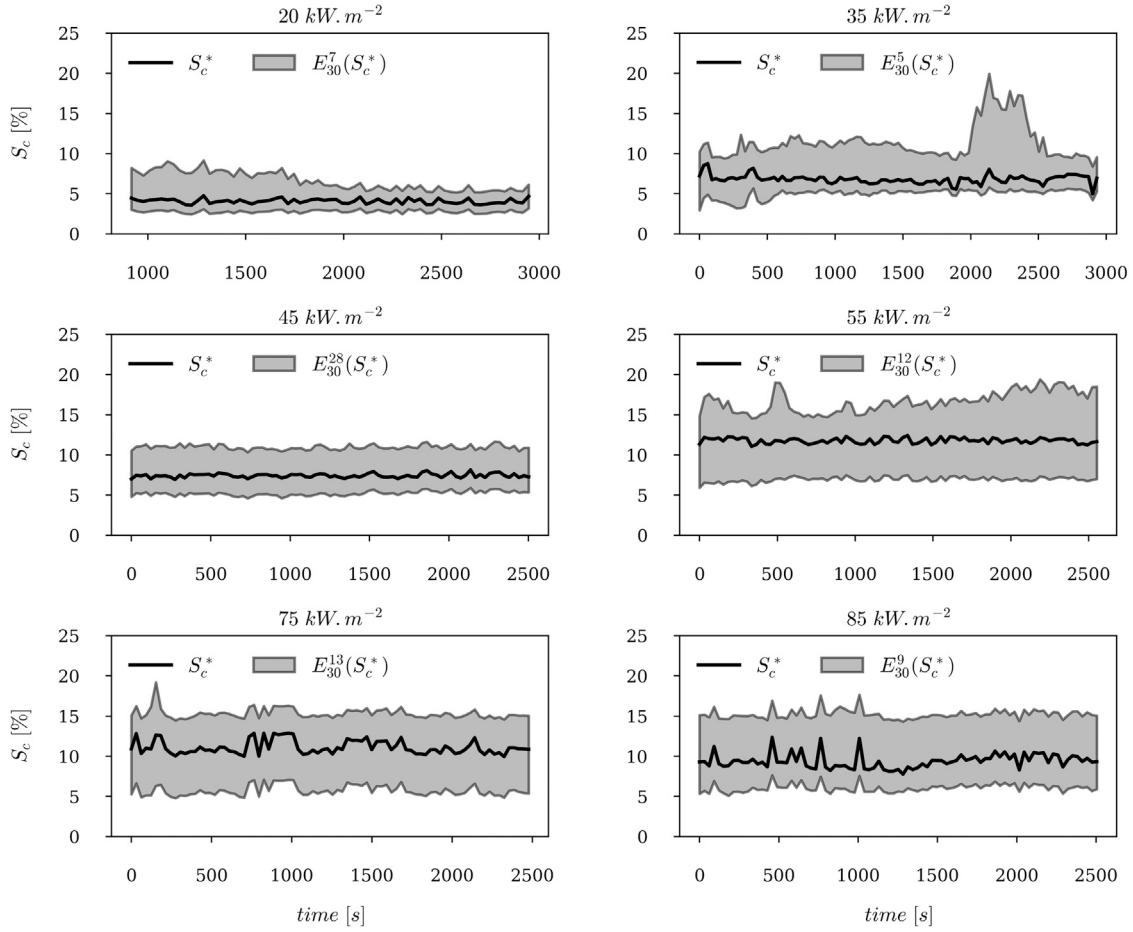


**Fig. 3.** Evolution of the mean crack ratio according to the imposed heat flux.

contours will be averaged over 30-second intervals. Consequently, the first data point in the forthcoming plots may be slightly biased due to the inclusion of a grain pattern. Nevertheless, this effect is negligible given the hundreds of data points considered in the analysis.

At $t = 72$ s, cracks are correctly detected, except along the right edge of the image. This is because a minimum area condition has been implemented (contour area greater than 20 pixels) to account for the presence of a crack. This criterion allows for the removal of ash-detecting contours that may appear during the test. As the exposure time increases from 72 to 729 s, the number of cracks decreases, but their width increases. At $t = 142$ s, five cracks were identified. The central crack, between $y = 20$ mm and $y = 40$ mm, consists of two horizontal cracks and a vertical crack connecting them. This vertical crack is shallower than the two horizontal cracks. As the exposure time increases, smoldering causes the vertical crack to disappear, as can be seen at $t = 792$ s.

In this study, three descriptors were selected to be examined over time: cracking ratio, crack length and number of cracks. The crack ratio, $S_c$, is defined as the sum of the area of each crack divided by the total area of the window of interest. The average characteristic crack length $L_c$, is obtained by dividing the perimeter ($P_c$) of each crack by two. Since the cracks depicted in the plan are elongated features, with a length significantly greater than the width, the calculation $L_c = P_c/2$ leads to an overestimation equivalent to approximately one width relative to the maximum length of a classic elongated crack. However, in the case of compound cracks, as shown in Fig. 1 at $t = 142$ s, the half-perimeter provides an accurate estimate of the total crack length. The average characteristic length at each time point was scaled by the width of the window of interest. Note that this dimensionless factor can produce values greater than 100% in cases involving compound cracks or single cracks larger than the window of interest. The final descriptor is the number of cracks, $N_c$. The temporal evolution of the descriptors is determined by calculating the most frequent value over a time interval of 30 s. For each time interval $\Delta t$, the probability density $p(\lambda)$ is constructed, where $\lambda$ is the class associated with the descriptor under study. The number of classes $\lambda$ at each interval is determined by the Freedman-Diaconis estimator. The most probable or peak value is $\lambda^*$ such as $p(\lambda^*) = \max(p(\lambda))$. The associated error is given by Eq. (1):

$$E_{\Delta t}^n(\lambda^*) = \begin{cases} +\sqrt{\frac{\sum_i p(\lambda_i)(\lambda_i - \lambda^*)^2}{\sum_i p(\lambda_i)}} & \text{if } \lambda_i > \lambda^* \\ -\sqrt{\frac{\sum_i p(\lambda_i)(\lambda_i - \lambda^*)^2}{\sum_i p(\lambda_i)}} & \text{if } \lambda_i < \lambda^* \end{cases} \quad (1)$$

where $i$ is the number of classes and $n$ is the number of tests. The choice to use the peak value rather than the mean is motivated by the fact that the distribution obtained at each $\Delta t$ interval is often off-center. Note that in the case of a Gaussian distribution, $E_{\Delta T}^n(\lambda^*)$ is identical to the standard deviation.

For 20 kW·m$^{-2}$ heat flux, the analysis of the infrared images starts from the moment when the entire surface is glowing, because unlike the other heat fluxes, which are higher, there is a significant time during which only drying and pyrolysis occur [3]. Fig. A.7 shows the transition from pyrolysis to surface glowing. This transition creates a significant contrast between the burning zone and the pyrolysis zone, which the algorithm recognizes as a crack. Consequently, a time $t_{glow}$ is defined for this heat flux, corresponding to the longest time for which the glowing of all experiments is established.

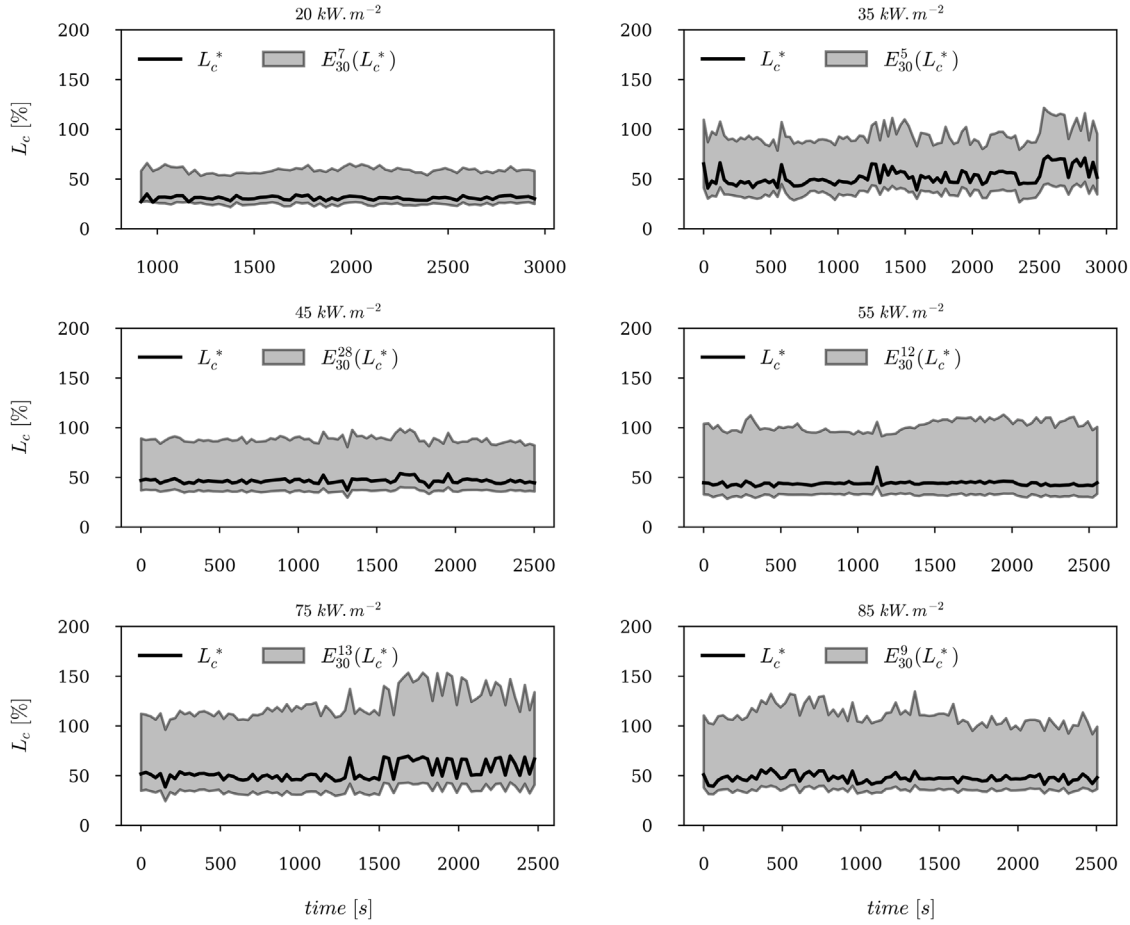


**Fig. 4.** Evolution of the mean characteristic length according to the imposed heat flux.

## 3. Results

### 3.1. Effect of the incident heat flux

For the 74 experiments carried out with the cone calorimeter in air, the sample self-ignited systematically for tests at 55 kW·m$^{-2}$ and for only 50% of the tests performed at 45 kW·m$^{-2}$ after one hour of exposure. At 20 and 35 kW·m$^{-2}$, there was no flaming ignition but only glowing. Fig. 2 shows the calculated charring parameters ($S_c$, $L_c$, and $N_c$) for three selected individual tests corresponding to three incident heat fluxes, $\dot{q}''_{inc} = 35, 55, 85$ kW·m$^{-2}$.

The 35 kW·m$^{-2}$ tests show a peak at the beginning of the experiment for the three studied parameters. This corresponds to the appearance of a large number of small cracks and is in accordance with the observations of Chu et al. [20]. These cracks quickly disappeared as the wood's surface began to pyrolyze and glow. The surface area of the cracks ($S_c$) remains constant at approximately 6% for one hour. However, increasing the imposed heat flux to 55 or 85 kW·m$^{-2}$ shows two regimes of $S_c$ over time: the first, where $S_c$ is around 12% and the second, where $S_c$ is around 8%. This regime change, caused by the disappearance of shallow cracks, occurs earlier with increasing heat flux as surface oxidation becomes more significant. The characteristic length ($L_c$) and the number of cracks ($N_c$) are related variables, as an increase in $L_c$ is accompanied by a decrease in $N_c$. Additionally, $L_c$ and $N_c$ fluctuate during the experiment. This is due to cracks' tendency to appear, move, split, merge, and partially or completely disappear over time. Thus, when two cracks merge, $N_c$ decreases, but $L_c$ increases. Conversely, when a crack dissociates, $N_c$ increases, and $L_c$ decreases. Regardless of the applied heat flux, $N_c$ varies between 3 and 9.

Fig. 3 shows the average surface crack ratio ($S_c$) and its uncertainty according to the heat flux. When averaged over several test runs, the crack ratio shows a constant trend over time, regardless of the applied heat flux. This observation suggests that the variations observed in individual tests — such as fluctuations in the crack ratio — are due to the natural variability of the experimental process. Consequently, the temporal evolution of the crack ratio can be characterized as statistically stationary. For a given heat flux, the average $S_c$ is nearly constant and appears to increase by 4.1% at 20 kW·m$^{-2}$ and up to 11.8% at 55 kW·m$^{-2}$. Table A.2 presents the time-averaged values of the descriptors over the entire duration of the test, bounded by the asymmetric upper and lower errors, calculated from the averages of the upper and lower bounds of the error $E$. Therefore the heat flux seems to be a factor that tends to increase the surface area of the cracked sample, especially above 35 kW·m$^{-2}$ (where solid combustion occurs rapidly). However, this trend is unclear since at a heat flux of 85 kW·m$^{-2}$, $S_c$ is about 9.4%, so the cracked area is smaller than tests at 55 kW·m$^{-2}$. Furthermore, even the standard deviations increases from 55 kW·m$^{-2}$, the dependence on the heat flux is small (20 kW·m$^{-2}$: $S_c = 4.1^{+2.5}_{-1.3}$%). Finally, for the range of heat flux studied, $S_c$ never seems to exceed 15%. Experimental results on self-extinction conditions for wood [6] suggest that larger cracks appear to release more pyrolysis gas locally, thereby maintaining the flame at that location. It can be inferred that a surface with small cracks would lead to self-extinguishing conditions, however this has not been proven quantitatively, and further testing is required to prove this.

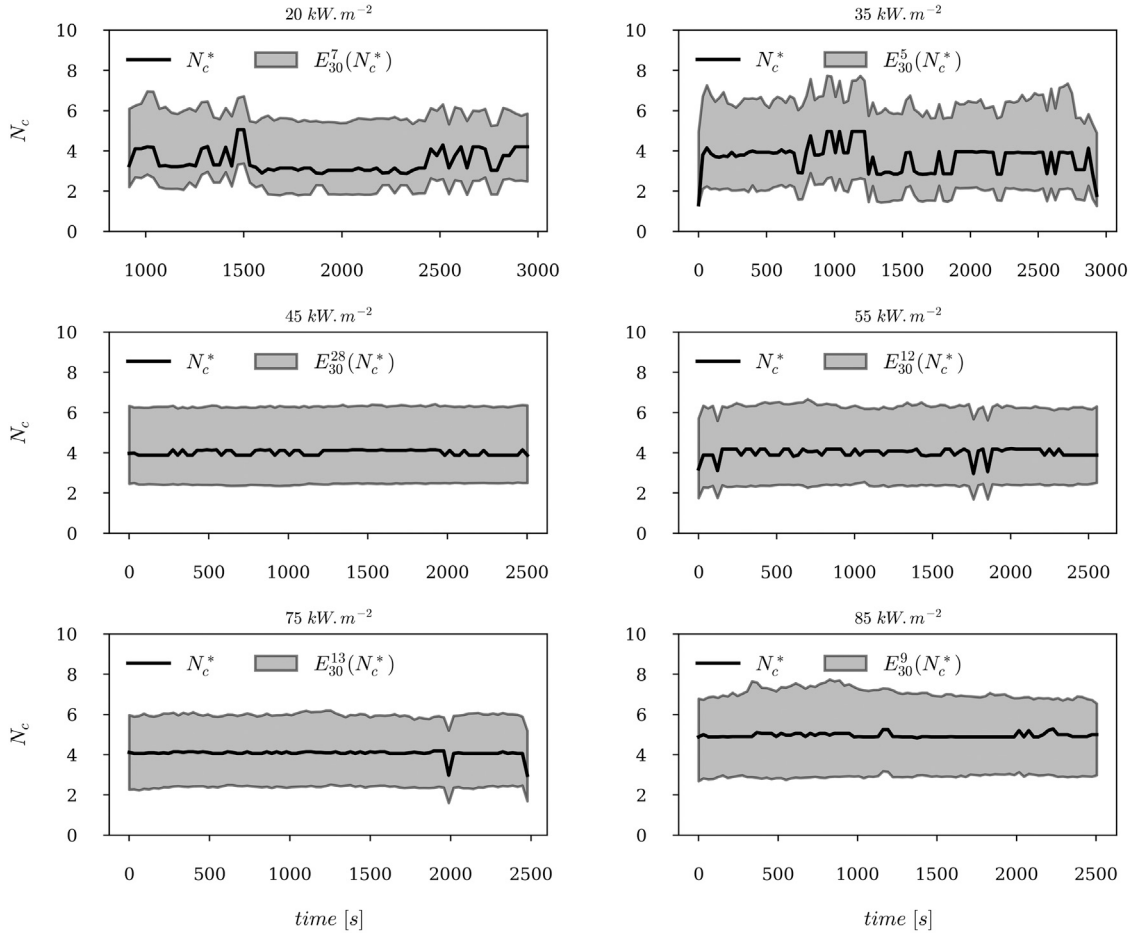


**Fig. 5.** Evolution of the mean number of cracks according to the imposed heat flux.

Fig. 4 shows the average characteristic length ($L_c$) and its uncertainty according to heat flux. The temporal evolution of the characteristic crack length also appears to follow a constant trend when averaged over several tests like for the cracking ratio. At 20 kW·m$^{-2}$, $L_c$ is lower at $L_c$ = 30.9%, increases to 52.5% at 35 kW·m$^{-2}$ and remains around this value up to 85 kW·m$^{-2}$ (Table A.2). Two regimes can be distinguished: one at low heat flux, where glowing and smoldering combustion occur over a long time, and one at high heat flux, where solid-phase or gaseous combustion occurs rapidly.

Fig. 5 shows the average number of cracks ($N_c$) and its uncertainty according to the incident heat flux. As with $S_c$ and $L_c$, the number of cracks averaged over the number of tests remains constant over time when the heat flux is fixed. The number of cracks is around 4 for the studied surface, regardless of the applied heat flux (Table A.2).

### 3.2. Effect of char oxidation

Fig. 6 illustrates the impact of oxygen on the crack ratio, characteristic length, and number of cracks in relation to the applied heat flux. Tests were performed in an inert atmosphere at 35 and 45 kW·m$^{-2}$ for 20 min and are labeled (Ar).

Under these experimental conditions, oxidation is negligible and the surface hardly regresses, in contrast to conditions under air. The videos show that, as soon as pyrolysis begins, the wood tends to crack rapidly. However, there is no disappearance or appearance of cracks during exposure to the heat flux. In other words, the cracks that appear remain throughout the test. Since less tests were performed, $S_c$, $L_c$, and $N_c$ are noisier for inert atmosphere tests, but the standard deviations are still in the same range as air tests and are considered satisfactory. At 35 kW·m$^{-2}$, the average $S_c$ varies from 4.9 under argon to 6.8 under air, and the average $N_c$ varies from 3.7 to 4.5. The trend is similar at 45 kW·m$^{-2}$. However, taking into account the errors in the averaged values shows that $S_c$, $L_c$, and $N_c$ are similar for the two environments. Regardless of the variable studied and for both heat fluxes, spruce cracking appears to be similar with or without the presence of oxygen. This means that the environment and surface char oxidation reactions are not the ruling factors in wood cracking. The diffusion of oxygen at the interface between the char layer and the surface causes oxidation and therefore the combustion of the char, but does not significantly increase the number or equivalent surface area of cracks. Finally, we hypothesize that the nature, morphology and internal stresses present in the material predetermine the cracking.

## 4. Conclusion

Although wood cracking influences the heterogeneous release of pyrolysis gases, its effect has not been clearly quantified yet. The introduction of statistical characteristics of the wood cracking during exposure to fire is important for accurately modeling its behavior especially for local phenomena such as ignition or flame extinction, since these are the areas where pyrolysis gases exit. Dynamic infrared imaging was used to monitor the evolution of cracking structures on the sample surface over time during the various phases of degradation. The study carried out on 81 tests in oxidizing and inert atmospheres

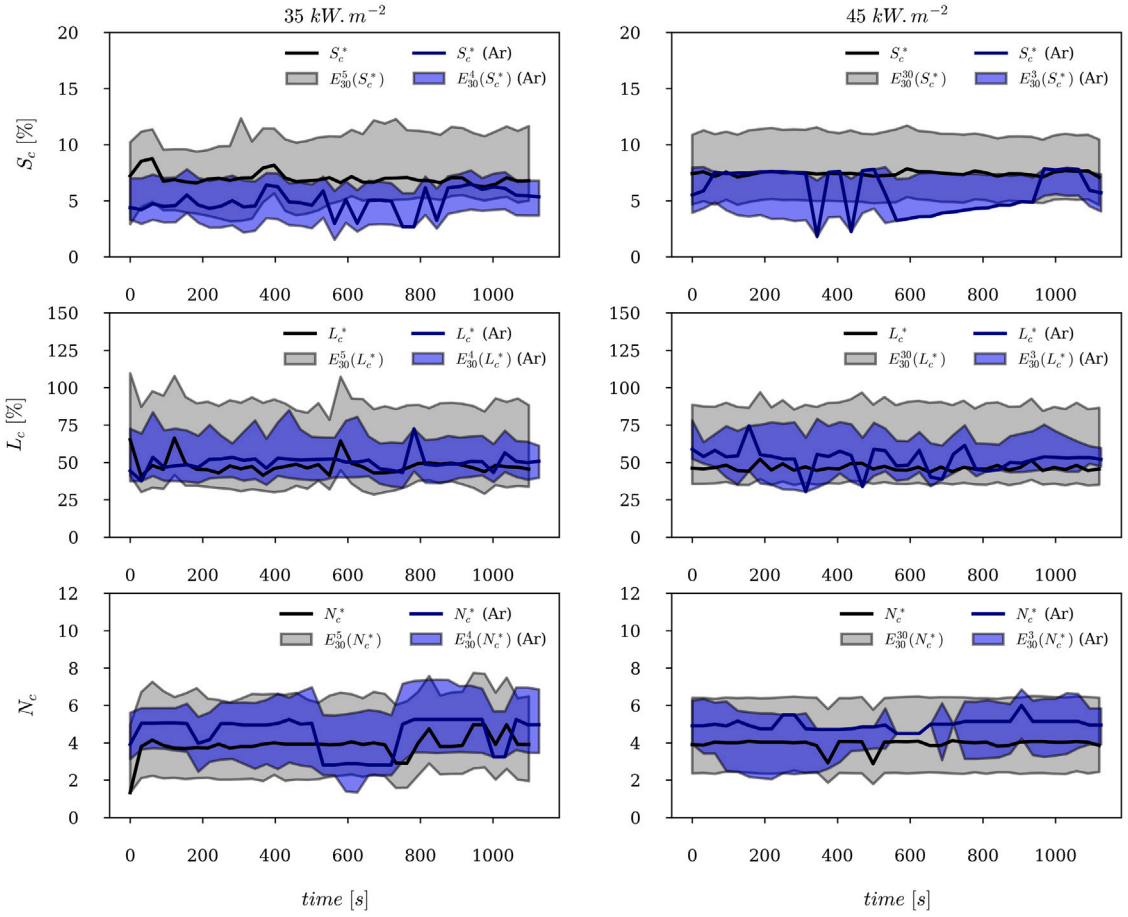


**Fig. 6.** Cracks ratio, characteristic length and number of cracks according on environmental conditions for two imposed heat fluxes.

at different heat fluxes, shows that the time-resolved determination of characteristic values ($S_c$, $L_c$, and $N_c$) makes it possible to separate two cracking regimes: low heat flux (under 20 kW·m$^{-2}$) and high heat flux (above 35 kW·m$^{-2}$). It was observed that the characteristic cracking values quickly reach stable values. This makes it easier to consider into a model, since the corresponding heterogeneity could be defined once and for all in a given case. The crack ratio tends to increase with heat flux ranging from 4.1% to 11.8%, although the standard deviations encompass these values. The number of cracks on the analyzed surface varies from 3.5 to 5. The results indicate that heat flux and surface oxidation reactions are not dominant factors governing wood cracking. Rather, the natural structure of the wood and the release of internal surface stresses through wood degradation might be the main causes of the number, area, and size of cracks.

## CRediT authorship contribution statement

**Boris Aguilar:** Validation, Methodology, Investigation, Formal analysis, Data curation, Conceptualization. **Pedro Reszka:** Writing – original draft, Validation, Supervision, Investigation. **Zoubir Acem:** Writing – original draft, Validation, Supervision, Data curation. **Pascal Boulet:** Writing – original draft, Visualization, Validation, Supervision, Formal analysis. **Gilles Parent:** Writing – original draft, Visualization, Validation, Supervision, Data curation, Conceptualization. **Lucas Terrei:** Writing – original draft, Methodology, Formal analysis, Data curation, Conceptualization.

## Declaration of competing interest

The authors declare that they have no known competing financial interests or personal relationships that could have appeared to influence the work reported in this paper.

## Acknowledgment

This work was partially supported by Universidad Adolfo Obáñez, through the programme Concurso Redes Para la Investigacíon 2025.

## Appendix

See Fig. A.7 and Table A.2.

**Table A.2**
Mean results for $S_c$, $L_c$ and $N_c$ with the positive ($E^+$) and negative ($E^-$) mean errors.

| Heat flux kW·m$^{-2}$ | $S_c$ % | $L_c$ % | $N_c$ – |
|---|---|---|---|
| 20 | $4.1^{+2.5}_{-1.3}$ | $30.9^{+28.1}_{-5.9}$ | $3.5^{+2.4}_{-1.2}$ |
| 35 | $6.8^{+4.7}_{-1.8}$ | $52.5^{+42.0}_{-16.1}$ | $3.7^{+2.7}_{-1.7}$ |
| 45 | $7.4^{+3.5}_{-2.2}$ | $46.5^{+41.7}_{-10.0}$ | $4.0^{+2.3}_{-1.6}$ |
| 55 | $11.8^{+4.9}_{-4.8}$ | $43.8^{+58.4}_{-11.5}$ | $4.0^{+2.3}_{-1.6}$ |
| 75 | $11.1^{+4.2}_{-5.4}$ | $54.0^{+69.0}_{-18.5}$ | $4.1^{+1.9}_{-1.7}$ |
| 85 | $9.4^{+5.8}_{-3.4}$ | $47.8^{+62.6}_{-11.8}$ | $5.0^{+2.1}_{-2.0}$ |

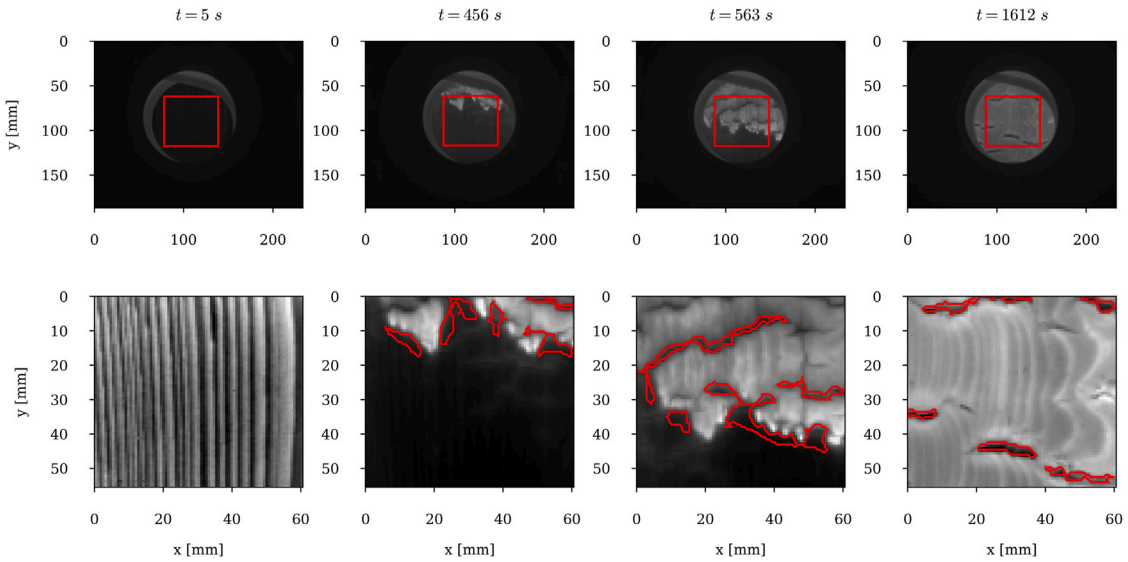


**Fig. A.7.** Infrared images and detection of the zone studied during the cracking of wood exposed to 20 kW·m$^{-2}$, where surface glowing is significant before cracks become noticeable.

## Data availability

Data will be made available on request.

## References


[1] D. Drysdale, An Introduction to Fire Dynamics, third ed., John Wiley & Sons, New York, 2011.

[2] N. Boonmee, J. Quintiere, Glowing ignition of wood: The onset of surface combustion, Proc. Combust. Inst. 30 (2) (2005) 2303–2310.

[3] L. Terrei, Z. Acem, V. Georges, P. Lardet, P. Boulet, G. Parent, Experimental tools applied to ignition study of spruce wood under cone calorimeter, Fire Saf. J. 108 (2019) 102845.

[4] J. Yang, A. Hamins, L. Dubrulle, M. Zammarano, Experimental and computational study on the glowing ignition of wood, Fire Mater. 47 (5) (2023) 638–650.

[5] Z. Zhang, P. Ding, S. Wang, X. Huang, Smouldering-to-flaming transition on wood induced by glowing char cracks and cross wind, Fuel 352 (2023) 129091.

[6] L. Terrei, Z. Acem, P. Lardet, P. Boulet, G. Parent, Study of wood self-extinguishment with a double sliding cone calorimeter, Fire Saf. J. 122 (2021) 103316.

[7] C. Bamford, J. Crank, D. Malan, The combustion of wood. Part 1, Proc. Camb. Philos. Soc. 42 (1946) 166–182.

[8] A. Galgano, C. Di Blasi, A volumetric reaction model for the combustion of moist wood exposed to moderate thermal irradiances, Fire Saf. J. 152 (2025) 104311.

[9] D. Baroudi, A. Ferrantelli, K.Y. Li, S. Hostikka, A thermomechanical explanation for the topology of crack patterns observed on the surface of charred wood and particle fibreboard, Combust. Flame 182 (2017) 206–215.

[10] I.S. Wichman, Y.T. Nguyen, T.J. Pence, A model for crack formation during active solid pyrolysis of a char-forming solid: Crack patterns; surface area generation; volatile mass efflux, Combust. Theory Model. 24 (5) (2020) 903–925.

[11] Y. Zhang, D. Behera, E. Madenci, Peridynamic modeling of thermal response and cracking in charring materials due to ablation, Eng. Comput. 40 (1) (2024) 343–365.

[12] D.K. Shen, S. Gu, K.H. Luo, A.V. Bridgwater, Analysis of wood structural changes under thermal radiation, Energy & Fuels 23 (2) (2009) 1081–1088.

[13] M.P. Conrad, G.D. Smith, G. Fernlund, Fracture of solid wood: A review of structure and properties at different length scales, Wood Fiber Sci. (2003) 570–584.

[14] K. Kwiatkowski, K. Bajer, A. Celińska, M. Dudyński, J. Korotko, M. Sosnowska, Pyrolysis and gasification of a thermally thick wood particle — Effect of fragmentation, Fuel 132 (2014) 125–134.

[15] K. Li, S. Hostikka, P. Dai, Y. Li, H. Zhang, J. Ji, Charring shrinkage and cracking of fir during pyrolysis in an inert atmosphere and at different ambient pressures, Proc. Combust. Inst. 36 (2) (2017) 3185–3194.

[16] K. Li, M. Mousavi, S. Hostikka, Char cracking of medium density fibreboard due to thermal shock effect induced pyrolysis shrinkage, Fire Saf. J. 91 (2017) 165–173, Fire Safety Science: Proceedings of the 12th International Symposium.

[17] T. Chu, C. Fan, C. Liu, S. Feng, Z. Wang, K. Liew, Effect of structural characteristics on charring shrinkage and cracking of densified wood under radiative heatings, Fire Saf. J. (2024) 104204.

[18] T. Chu, Z. Wang, S. Lin, C. Fan, Investigation on the char crack growth of densified wood, Eng. Fract. Mech. 314 (2025) 110697.

[19] A. Rinta-Paavola, A. Ferrantelli, S. Hostikka, Experimental observation of crack formation on surface of charring timber, Fire Saf. J. 148 (2024) 104231.

[20] W. Chu, J. Fang, R. Zhou, Y. Wang, A novel methodology to gauge and quantify the surface cracks of burning timber, Fire Technol. (2025) 1–12.

[21] L. Terrei, D. Zeinali, Z. Acem, V. Marchetti, P. Lardet, P. Boulet, G. Parent, Experimental study of spruce wood reaction to fire in single burning item test, J. Fire Sci. 40 (4) (2022) 293–310.

[22] L. Terrei, G. Gerandi, H. Flity, V. Tihay-Felicelli, Z. Acem, G. Parent, P.-A. Santoni, Experimental and numerical multi-scale study of spruce wood degradation under inert atmosphere, Fire Saf. J. 130 (2022) 103598.

[23] A. Mariam, H. Flity, L. Terrei, A. Zoulalian, R. Mehaddi, P. Girods, Y. Rogaume, An alternative wood pyrolysis model based on TGA and cone calorimeter tests, Thermochim. Acta 731 (2024) 179646.

[24] G. Parent, Z. Acem, S. Lechêne, P. Boulet, Measurement of infrared radiation emitted by the flame of a vegetation fire, Int. J. Therm. Sci. 49 (3) (2010) 555–562.

[25] L. Terrei, Z. Acem, V. Marchetti, P. Lardet, P. Boulet, G. Parent, In-depth wood temperature measurement using embedded thin wire thermocouples in cone calorimeter tests, Int. J. Therm. Sci. 162 (2021) 106686.

[26] L. Terrei, H. Flity, O. Ikhou, G. Trohel, J.L. Torero, Z. Acem, G. Parent, Effect of the wood species on the fire behavior in vertical orientation, Fire Saf. J. 148 (2024) 104234.